JOURNAL OF MATERIALS SCIENCE 17 (1982) 1171–1186

Radial distribution functions of non-crystalline polymers and their application to the structural analysis of PMMA

J. R. WARING*, R. LOVELL, G. R. MITCHELL, A. H. WINDLE
Department of Metallurgy and Materials Science, University of Cambridge, Pembroke Street, Cambridge, UK

The use of Radial Distribution Functions (RDFs) in the determination of the structure of non-crystalline polymers is briefly reviewed. Particular aspects of the procedure for preparing RDFs from X-ray scattering are discussed in detail; namely the employment of an energy dispersive detector to remove the Compton component of the scattered X-rays and the application of the method of sampled transforms. A RDF is presented for atactic polymethylmethacrylate (PMMA) and its precision and reliability are discussed. It is analysed by comparison with RDFs calculated from computer-generated atom co-ordinates for isolated lengths of PMMA chains in different conformations. Methods are introduced by which the calculated RDFs are smeared to account for random disorder in the real chain and normalized so that, despite the finite range of the model, they can be immediately compared with the difference RDF which is directly obtained by transforming the data. Comparison between experimental and calculated RDFs shows that reasonable agreement is only obtained for a very limited range of conformations corresponding to sequences of backbone bond rotation angles of (10°, 10°, −10°, −10°) and the bond angles alternately 110° and 128°. The form of the RDF appears very sensitive to important aspects of the molecular structure. The results both confirm and refine an earlier proposal from this laboratory which was based on comparisons between experimental and calculated functions in reciprocal space.

1. Introduction

1.1. Radial distribution functions of non-crystalline polymers

X-ray diffraction from non-crystalline materials produces diffuse peaks which are commonly analysed in terms of Radial Distribution Functions (RDFs). Such functions are generated by Fourier transformation of the reduced data and are the spherically averaged distributions of inter-electronic (or alternatively interatomic) vector lengths within the material. The usefulness of a RDF stems from the fact that interpretation is more straightforward than the corresponding scattering function, for it obviously cannot contain more information than the diffraction pattern from which it is derived. However, the analytical process does tend to enhance the scattering information due to shorter range correlations at the expense of that corresponding to larger distances. For example, with organic polymers the covalently determined first and second nearest-neighbour distances show up as clear peaks in the RDF, whereas on the diffraction pattern, they correspond to long wavelength oscillations which are not especially apparent. On the other hand diffuse diffraction peaks which occur at lower angles and are not particularly intense, such as that at $s = 7\,\text{nm}^{-1}$ in the pattern from polystyrene [1] ($s = 4\pi \sin\theta/\lambda$, where θ is the Bragg angle and λ is the wavelength of the X-rays) do not lead to any distinctive

*Present address: British Railway Technical Centre, London Road, Derby, UK.

0022–2461/82/041171–16$04.42/0

features on the RDF even though they may bear important structural information.

The first RDF of an amorphous polymer was published by Simard and Warren [2] for natural rubber in 1936. Later, in 1954, Bjørnhaug *et al.* [3] calculated RDFs of several non-crystalline polymers from photometric intensity measurements on X-ray films. The expected 0.15 nm and 0.25 nm repeats (representing the fixed distances between first and second nearest-neighbours joined by covalent bonds) were clearly shown. The authors suggested that peaks at distances greater than 0.5 nm were due to inter-molecular distances.

Since this comparatively early work, RDFs have been published for polystyrene [1], polycarbonate [4] and polyethylene terephthalate [5, 6]. The polyethylene melt has also been analysed on the basis of both X-ray data [7, 8] and electron diffraction measurements [9, 10]. It is noteworthy that the two papers dealing with RDFs derived from electron diffraction, which tend to have better resolution for distances less than 0.5 nm, are able to present firmer (although conflicting) proposals regarding intramolecular order.

For RDFs from polymer glasses there have been several attempts to correlate the functions with interatomic distances corresponding to particular conformational models of isolated molecules [4, 7, 9]. Although some of these results do provide structural indications, it is perhaps fair to say that they are not totally convincing.

1.2. The scope of this paper

As part of a broadly based programme to explore the structure of non-crystalline polymers, we have set out to optimize the procedure of RDF analysis in an effort to explore its full potential as a structural technique. As a result of a critical examination of the experimental, analytical and interpretive stages of the complete procedure, several developments have been made. Of these, the use of an energy dispersive detector in data collection and the introduction of the method of sampled transforms to reduce termination error have already been described [11, 12]. In this paper we examine other variations in the RDF procedure with the objective of achieving the maximum resolution while ensuring freedom from spurious detail. We have chosen to work with atactic polymethyl methacrylate (a-PMMA) but the results are generally applicable, particularly to other non-crystalline polymers [13]. The significant question as to whether RDFs, even when produced with great care, are sensitive enough to minor changes in molecular conformation to be a valid tool in structural analysis is explored by comparisons with RDFs calculated from computer-built models of isolated molecules in different conformations. The work demonstrates that RDFs are indeed sensitive to small conformational changes.

For PMMA, we have previously made detailed proposals of the conformational structure based on comparisons made in reciprocal space [14, 15]. However, the generation of a trustworthy RDF of reasonable resolution now enables us to check these proposals in real space and to determine whether the fact that RDFs usually show more peaks than a scattering function can enable a finer differentiation to be made between different structural models. In short, we use the RDF both to check and refine our existing model.

2. Development of RDF analysis for non-crystalline polymers

A brief account of the established RDF procedures is given in Appendix 1. In this section we point to some of the difficulties which are particularly apparent in RDF analysis of polymers and outline the method of sampled transforms which overcomes several of the problems.

The transform integral used to generate radial distribution functions must operate between the limits zero and infinity. Experimental data however are necessarily terminated at a finite value of s, i.e., s_{max}. The straightforward application of many transform (computer) routines will calculate RDFs at intervals which can be varied at will, and there is a tendency to reduce these intervals to a minimum to facilitate the drawing of smooth curves. The transform integral, however, effectively operates on the data as if they run from $s = 0$ to infinity but step artificially to zero at s_{max}. The transform of the unreduced data in Fig. 1a will contain a dominant ripple known as termination error. The production of an RDF requires that the data is s-weighted before transforming which has the effect of making the step at s_{max} relatively more prominent. The resultant ripple on the RDF can totally swamp any useful information.

Reduction of the corrected data to give the interference function (Fig. 1b) by subtracting a suitably scaled $\sum_i f_i^2$ function together with the

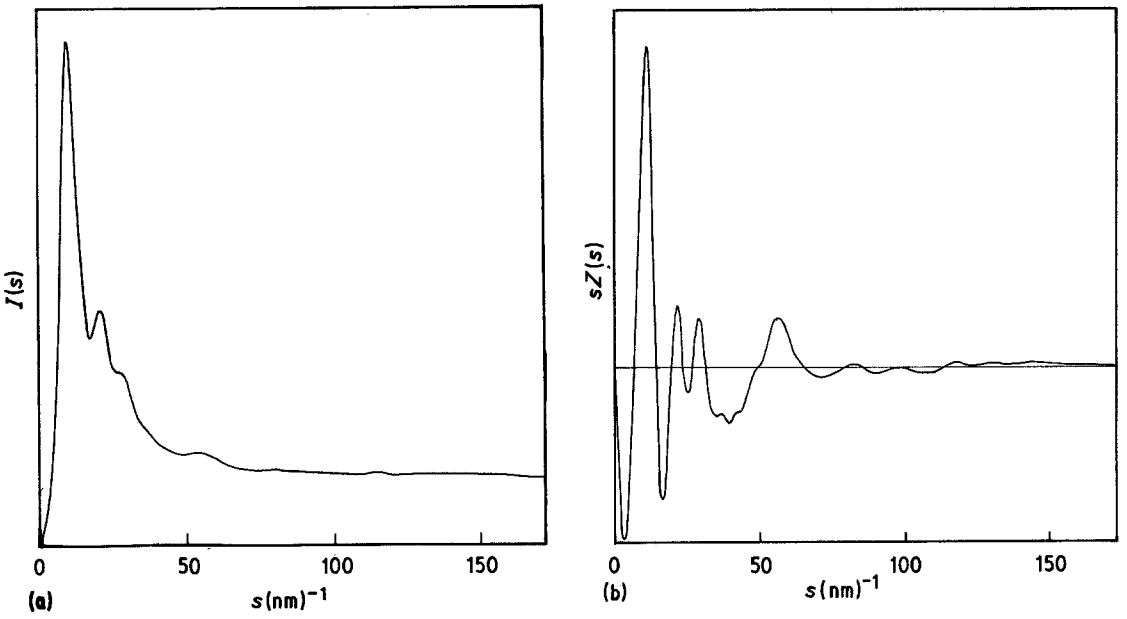

Figure 1 Showing (a) plot of the fully corrected X-ray intensities for PMMA as a function of scattering vector, s, where $s = 4\pi \sin\theta/\lambda$, (b) an interference function prepared from the intensity plot by normalizing to the independent scattering (Σf^2 + Compton component).

Compton component will have the effect of considerably reducing the step at s_{max} and thus the unwanted ripple on the RDF. In fact, in the production of RDFs of polymers where the main interest focusses on the information at medium and high values of r, the most important purpose served by normalization is the reduction of termination ripple. The removal of intra-atomic distances which prevail at values of r less than 0.2 nm and the distortion due to the presence of Compton scattering assume secondary importance.

Perfect normalization depends on an absolutely precise knowledge of $\sum_i f_i^2$, and the correct calculation of the Compton component. The latter, in particular, is especially difficult owing to the complex interactions between absorption and multiple-scattering corrections. Even if it were possible, the interference function may still be non-zero at s_{max}, so a termination discontinuity can remain and with it the possibility of spurious information on the RDF. Sharpening, by division of the interference function by $(\sum_i f_i)^2$, further exaggerates any step at s_{max} and therefore enhances the spurious ripple. Control of such temination error, particularly on atomic RDFs, has often been achieved by smoothing or damping. But when it is borne in mind that the interference function is damped by multiplying it by a function which is often very similar to the sharpening denominator $(\sum_i f_i)^2$, the limited value of the approach becomes apparent. This argument was presented by Wignall and Longman [4], who have also used a technique [16] for the reduction of termination error by selecting s_{max} at a value where the interference function crosses zero. This method, while reducing the ripples in the RDF due directly to the step at s_{max} will tend to enhance those resulting from the discontinuity in the first and higher derivatives of the interference function. The net result however is advantageous.

The method of sampled transforms introduced into RDF analysis by Lovell, Mitchell and Windle [12] largely overcomes the problem of spurious ripples due to termination error. In effect the transform is only calculated at values of r which correspond to sine waves of wavelengths that are particular factors of s_{max}. For the case of an interference function terminated at an arbitrary point (i.e. not at a node), the RDF is best calculated at values of

$$r = (2n + 1)\pi/2s_{max} \qquad (n = 0, 1, 2 \ldots)$$

with subsequent averaging over each successive three-point sequence, although the averaging does reduce the resolution in the RDF. The use of sampled transforms has one significant advantage: a termination step in the interference function at s_{max}, irrespective of its origin, will not in itself

cause misleading or swamping ripples. There will of course still be limited resolution on account of the missing scattering information beyond s_{max}. Very bad normalization will give rise to a peak (positive or negative) between 0 and 0.1 nm which may have second or third harmonics, but in general where a reasonable level of normalization has been obtained the RDF will be no more than slightly distorted. An additional advantage of sampled transforms is that the spacing of the calculated points on the RDF gives a useful indication of the resolution to which one is entitled, on the basis of the particular range of s available.

It can be shown that the RDF generated using a sampled transform is not significantly affected by the deliberate introduction of bad normalization, and even in the extreme case of no normalization the important features of the RDF at medium r and above are still apparent. We have employed the sampled transform method for the generation of the RDF of PMMA, not because it removes the onus of reducing the data so as to produce the best possible interference function, but because it does not exaggerate the deficiencies which are bound to be present even in the best interference function.

For polymers, the RDF shows sharp maxima corresponding to covalent-bond-determined nearest and next-nearest neighbour distances. This information is of little value, as it can be derived directly from a knowledge of the chemical structure of the molecule. However, under some circumstances it can tend to swamp peaks due to short correlations which are conformationally sensitive (e.g. third nearest-neighbour distances). When this occurs it is advantageous to remove the dominant covalently determined peaks by normalizing the data to a Σf^2 function modulated by the calculated interference corresponding to the chemically defined distances. This procedure is not in fact used in the RDFs presented in Section 3.2, but is described and illustrated in Appendix 2.

3. The RDF of PMMA

3.1. Experimental method

The data from PMMA (ICI Perspex) were collected using a Philips horizontal diffractometer (PW 1380), a molybdenum target tube and parafocussing symmetrical reflection geometry. The detector was a Si(Li) crystal (KEVEX) which, combined with a multichannel analyser, enabled the Compton component of the radiation to be separated reliably. The method developed to achieve separation and further experimental details are published elsewhere [11]. The data for coherent scattering were smoothed to remove the statistical scatter using the method of fitted cubic splines [17] and then interpolated onto an s scale (where $s = 4\pi \sin\theta/\lambda$).

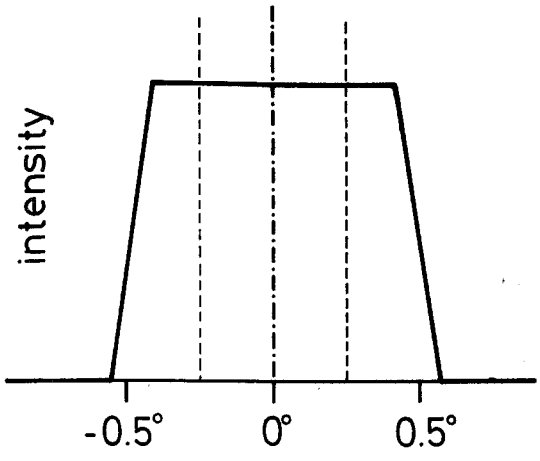

Figure 2 Form of beam profile at the specimen, used in the absorption correction, determined for nominal half degree slits.

As no monochromator was employed the correction for polarization was particularly straightforward. The correction for absorption in the reflection geometry was not so simple. The method employed was a development of that due to Milberg [18] who calculated analytical expressions for the absorption correction for an infinite sheet sample. We numerically integrated over the illuminated volume, which varies as a function of diffraction angle and, of course, slit geometry. The linear absorption coefficients were calculated from mass absorption coefficients in International Tables [19]. The fact that Compton Scattering was removed experimentally meant that the linear absorption coefficient could be taken to apply to the MoKα wavelength alone. The X-ray intensity distribution across the surface of the specimen was determined experimentally by measuring the diffraction intensity from a particularly narrow specimen as a function of its off-axis position in the symmetrical plane. For the purposes of the calculation the profile was approximated by the trapezium form of Fig. 2. The nominal width corresponding to the 0.5° slits used is shown by the vertical lines.

For organic materials the calculation of multiple scattering is particularly complicated as it is

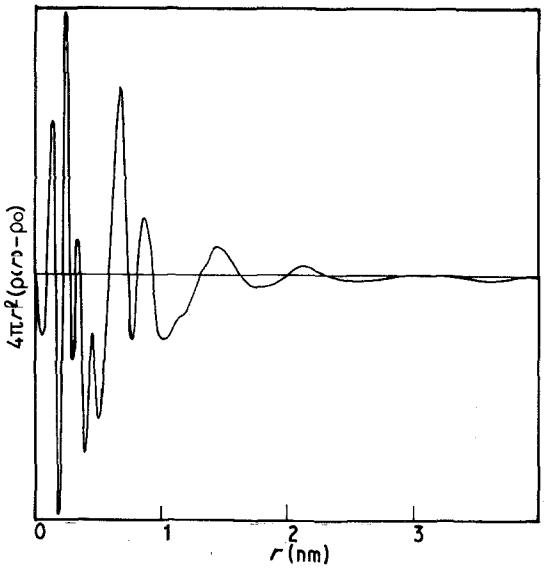

Figure 3 Atomic RDF, $(4\pi r^2(\rho(r)-\rho_0))$, calculated from the data of Fig. 1.

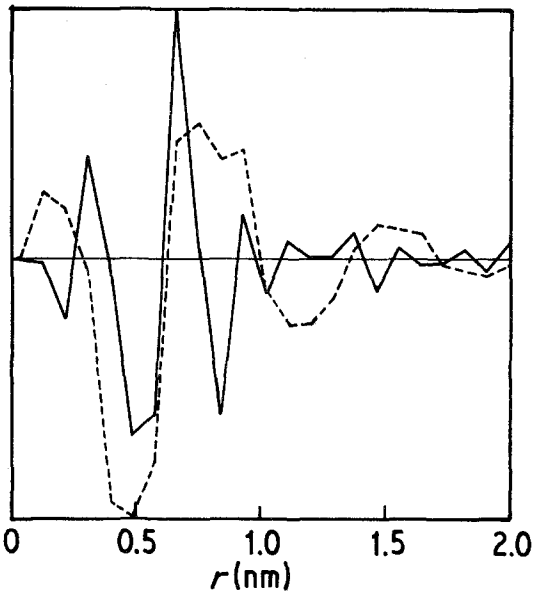

Figure 4 Meridional (——) and equatorial (-----) sections of the cylindrical distribution function determined from an oriented sample of PMMA.

necessary to consider the interaction of multiple scattering events with the coherent to non-coherent (Compton) events [11]. In principle, correction equations of the type developed by Warren and Mozzi [20] can handle this interacting situation; however, they will need to be extended to account for specimens of finite thickness before they are readily applicable to this work. But calculations after [20] show that at least 99% of the doubly scattered radiation will be incoherent [11], due mainly to the fact that the scattering cross-section is much less for the elastic case than it is for the Compton one. The useful consequence of this result is that if the incoherent component of the scattered radiation is removed experimentally, as it has been in the current work, then the vast majority of double scattering goes with it [11]; indeed to such an extent that the multiple scattering correction is no longer really necessary.

3.2. The RDF

The atomic RDF for PMMA is plotted in Fig. 3. It is expressed as a radial density function, $4\pi r^2(\rho(r)-\rho_0)$ and has been calculated from the interference function using the method of sampled transforms. Beyond the peaks at 0.15 nm and 0.25 nm, corresponding to distances fixed by covalent bonds, the main features are peaks at 0.67 nm and 0.92 nm which appear in the previously published RDF of PMMA [3]. However, the resolution achieved enables additional features to be resolved in the 0.3–0.6 nm region. Cylindrical distribution functions (CDF) derived using the scattering from oriented a-PMMA [21] show that the 0.67 and 0.92 nm peaks are intra-chain in origin, although they are superimposed on a broader inter-chain peak at around 0.8 nm. This peak is the first component of a damped ripple which is the typical manifestation of inter-chain correlation [13] in a polymer RDF. The peaks at 0.33 and 0.47 nm are also intra-chain. It is this region of the RDF which is particularly sensitive to small conformational changes, as is demonstrated in Section 5 below.

Fig. 4 is a plot of the equatorial and meridional sections of the CDF and clearly illustrates that the 0.67 and 0.92 nm correlations are along the direction of the molecular axis. (The 0.33 and 0.47 nm peaks are not resolved in this plot which shows an "electronic" function.)

4. Precision and reliability of the RDF

A major difficulty in comparing experimentally determined RDFs with those from models stems from having to know which of the more minor peaks can be taken as genuine. In other words, it is important to know the error limits before any RDF is used for structural predictions.

Errors are introduced at each stage in the experimental and analytical procedure. We have however set out to evaluate the consequences of the more important errors for the RDF of PMMA.

The types of error introduced have been dis-

cussed by several authors [22–25] together with detailed examination of the errors due to instrumental effects [26] smoothing [17], small-angle scattering [27] and scaling errors [28].

4.1. Distortion of RDF due to statistical uncertainty in the data

Short wavelength random fluctuations in the data due to counting statistics cause somewhat similar fluctuations on the RDF [17, 22]. Konnert and Karle [24] give an approximate relationship for the variance in the RDF ($G(r)$), $\sigma'^2(r)$, produced by random errors on the $sZ(s)$ curve:

$$\sigma'^2[rG(r)] \simeq \sum_s \left[\frac{2r}{\pi}\sigma(s)\sin rs\right]^2, \qquad (2)$$

where $\sigma(s)$ is the standard deviation in the interference function, and $sZ(s)$ is the s-weighted reduced intensity function.

The various $\sigma(s)$ may be obtained by analysis of the raw intensity values [25] and weighted with the appropriate factors. Although the magnitude on the noise (apart from the multiplication correction factor) is unchanged by the data correction procedure, the data values themselves are considerably altered by the subtraction of the independent scattering. Hence the signal-to-noise ratio in the interference function is particularly enhanced at high s values where the observed scattering is predominantly independent in nature. The effect of the noise may be greatly reduced by the use of an appropriate smoothing procedure [17].

Since the raw intensity curve at high s values contains only broad shallow peaks, the high-frequency noise component may be heavily smoothed and thus compensate for the noise enhancement due to the intensity reduction process. We have found the computer smoothing routine discussed by Dixon *et al.* [17] to be well suited for this procedure.

4.2. Distortions at low values of r

Incorrect compensation for the effects of multiple scattering, absorption and the incoherent component tends to produce errors in the interference functions which vary smoothly with s. As a result they will only upset the RDF at low values of r. For polymers, both the correct position and relative areas of the peaks near 0.15 and 0.25 nm can be taken as an indication that these errors are reduced to levels where they will not distort the structurally more important information at higher levels of r. Comparisons between the RDF and the function $4\pi r^2\rho_0$ at very low values of r can be used as a yet more stringent test for the presence of this class of error.

4.3. Ripples due to termination error

Unlike the previous errors, termination error, which at its worst can totally swamp a RDF in short-wavelength ripples, can be almost eliminated by making straightforward changes to the analytical procedure. The method of sampled transforms has been employed in this work.

4.4. Evaluation of errors

It is not possible to calculate the forms of error, other than that derived from statistical sources, with any degree of confidence. If there is doubt as to any feature in a RDF, the best method of checking its validity is to smooth it out and back-transform the function so as to reconstitute a modified interference function and thence a set of "decorrected data". Comparison with the original scattering data will show the features which correspond to that removed from the RDF and indicate whether they can be considered significant. There are in addition several general guidelines in Appendix 3.

5. Calculations of RDFs of model structures

5.1. General

We have concentrated on modelling single chains since the sharpest feature in a RDF of a polymer come from distances within the chains. Modelling of multiple-chain systems can only be easily carried out for parallel packing of straight chains or regular helices. The general problem of modelling the packing of curved or highly irregular chains is yet to be solved, although some success has been obtained with simple systems [29, 30]. We now describe how a model RDF can be calculated from a single chain in the form for easiest comparison with experimentally determined RDFs.

The first stage of the procedure is the calculation of the atomic co-ordinates for a length of molecule using a computer chain-building routine. Bond lengths and side-group conformations are set to fixed values, the desired chain conformation being specified by backbone bond angles and rotation angles. For PMMA the fixed values were those used by Sundararajan and Flory [31] with the ester sidegroup planar with the O–CH_3 bond *cis* to the C=O bond.

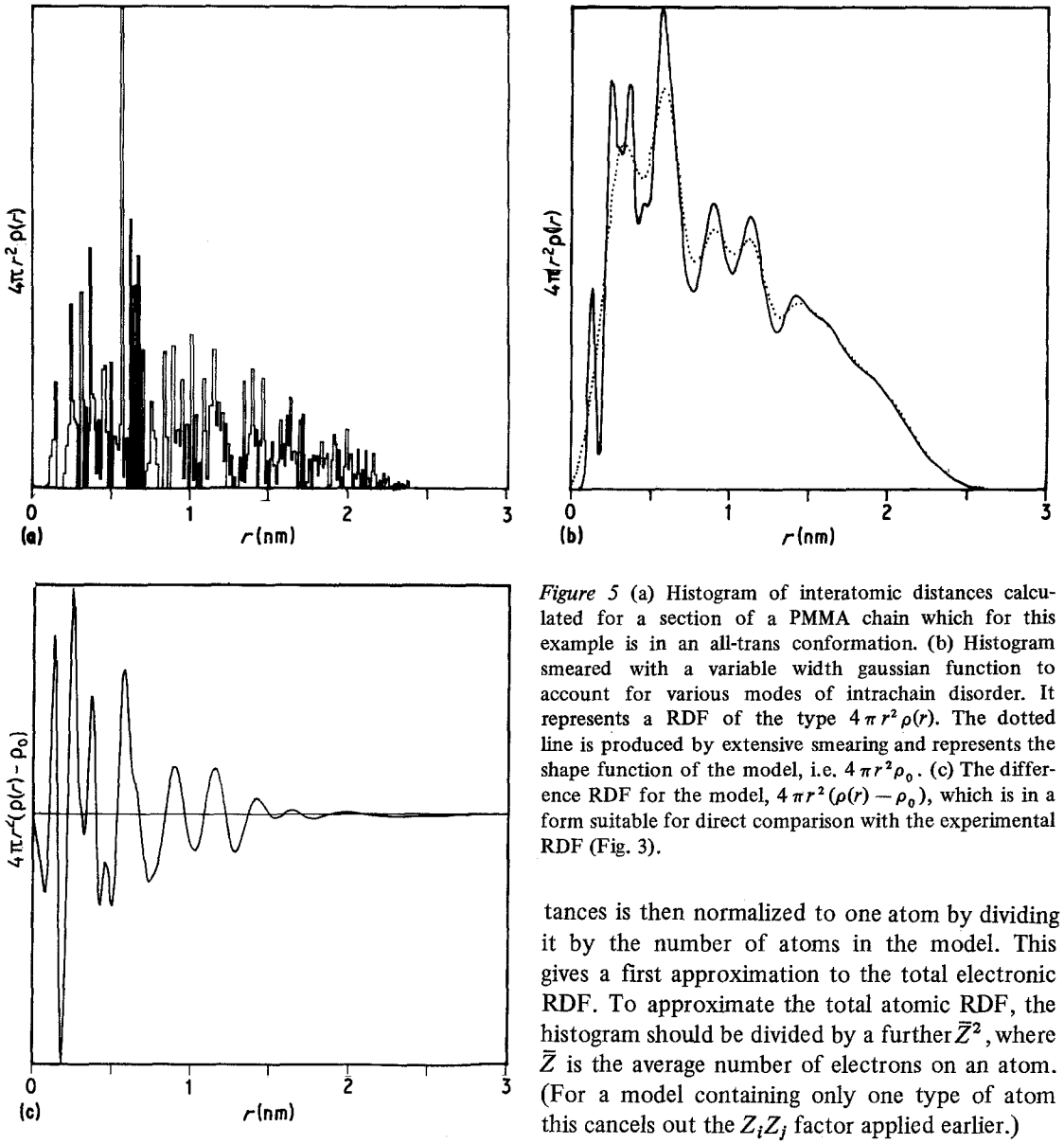

Figure 5 (a) Histogram of interatomic distances calculated for a section of a PMMA chain which for this example is in an all-trans conformation. (b) Histogram smeared with a variable width gaussian function to account for various modes of intrachain disorder. It represents a RDF of the type $4\pi r^2\rho(r)$. The dotted line is produced by extensive smearing and represents the shape function of the model, i.e. $4\pi r^2\rho_0$. (c) The difference RDF for the model, $4\pi r^2(\rho(r)-\rho_0)$, which is in a form suitable for direct comparison with the experimental RDF (Fig. 3).

The length of chain which is built depends not only on the maximum distance, r_{max}, out of which the RDF is to be calculated, but also on the regularity of the chain. A longer chain is needed for a highly irregular conformation to ensure that a representative sample of the different conformations is obtained.

The interatomic distances, r_{ij}, are calculated from the atomic co-ordinates, each distance being weighted with Z_iZ_j, where Z_i is the number of electrons on the ith atom. This is necessary since, even in sharpened RDFs derived from X-ray (or electron) scattering, the peaks are weighted by these factors. The histogram of interatomic distances is then normalized to one atom by dividing it by the number of atoms in the model. This gives a first approximation to the total electronic RDF. To approximate the total atomic RDF, the histogram should be divided by a further $\bar{Z}^2$, where $\bar{Z}$ is the average number of electrons on an atom. (For a model containing only one type of atom this cancels out the Z_iZ_j factor applied earlier.)

The histogram (Fig. 5a) differs in three distinct ways from experimental RDFs. Firstly, it has much sharper features than the experimental RDF. Secondly, it only has positive (or zero) values and approximates to a total RDF, $4\pi r^2\rho(r)$, rather than the reduced RDF, $4\pi r^2(\rho(r)-\rho_0)$, usually derived from data. Thirdly, it decays to zero at r_{max}, the maximum dimension of the model.

We now show how to modify the histogram to give a model RDF in a form similar to the experimental one.

5.2. Peak broadening

There are a number of reasons why a RDF derived from experiment has broader peaks than

those in the model RDF:

(a) The finite range of the scattering vector, s, limits the resolution to π/s_{max}, which is approximately 0.02 nm for $s_{max} = 150\,nm^{-1}$. No real features sharper than this limit can appear in an experimental RDF [12].

(b) Thermal motion broadens the peaks, particularly for the third and more distant neighbours. The different modes possible within polymer chains are (in increasing order of softness) (i) bond stretching, which affects all bonded distances, (ii) bond angle distortions, which affect atoms separated by two or more bonds, (iii) torsional oscillations, which affect atoms separated by 3 or more bonds.

(c) In an electronic RDF, each interatomic distance is smeared by the electron distributions of the two atoms.

There are various ways that these effects can be incorporated in model RDFs:

(a) The limited resolution could be simulated by calculating the scattering from the model using the Debye formula [32] and then transforming back to the RDF using the same s_{max} as for the data. However, comparison between calculated and experimental scattering would be more straightforward than transforming back. Alternatively, the resolution in the model RDF could be reduced by convolution with a peak-broadening function of constant width. The form of this function should take account of any damping function applied to the scattering before transformation [32–34].

(b) The most satisfactory method of introducing the effects of thermal motion is to build the model chain with these included, i.e., to assign values of bond lengths and angles randomly distributed within a range comparable with that expected for thermal motion. Alternatively, a peak-broadening function with a width increasing with r, could give a good approximation to the effects of thermal motion. This is the method adopted here.

(c) Ideally, to take account of the electron distribution of the atoms, each pair distribution function should be broadened with the convolution of the two atoms before all the pair distribution functions are combined to give the RDF. However, since the widths of the electron distributions of most of the atoms in polymers are similar, a single broadening function is adequate. This broadening is not, of course, included in the structural analysis below since comparison is made with atomic RDFs.

To model the first two types of broadening as simply as possible, we have adopted a Gaussion broadening function with a standard deviation, σ, given by

$$\sigma^2 = \sigma_0^2 + \sigma_1^2 r^2 \quad \text{where } \sigma_0 = 0.02\,nm \text{ and } \sigma_1 = 0.008\,nm. \tag{3}$$

These figures were chosen to give the RDFs the same general appearance in terms of the width and relative weights of peaks as is typical of experimental RDFs. Fig. 5b shows the effect of smearing the histogram of Fig. 5a using this function.

5.3. Reduction of model RDF

By subtracting a suitable function of r from the broadened histogram, we can obtain a distribution function which oscillates about the horizontal zero axis and is thus directly comparable with the reduced RDF. The problem is to find the correct function to substrate. In general, this may be written as $4\pi r^2 \rho_0 \gamma_0(r)$ where $\gamma_0(r)$ is the self-convolution of a volume with the same size and shape as the model. This shape function $\gamma_0(r)$ is used in the theory of small-angle scattering [19, 35] where it is called the characteristic (or correlation) function. It is unity at $r = 0$ and decays to zero at $r = r_{max}$, and although its behaviour at small r is given by [35]

$$\gamma_0(r) = 1 - \frac{Sr}{4V}, \tag{4}$$

where S is the surface and V is the volume of the model, a simple expression for $\gamma_0(r)$ can only be derived in a few special cases.

For a very large model with dimensions in all directions that are much greater than needed in the RDF, we may take $\gamma_0(r) = 1$ and hence subtract $4\pi r^2 \rho_0$ from the histogram.

For a spherical model of radius R [35]

$$\gamma_0(r) = \left(1 - \frac{r}{2R}\right)^2 \left(1 + \frac{r}{4R}\right), \tag{5}$$

whereas, for a cubic model of side L, [36, 37]:

$$\gamma_0(r) = 1 - \frac{3}{2}\left(\frac{r}{L}\right) + \frac{2}{\pi}\left(\frac{r}{L}\right)^2 - \frac{1}{4\pi}\left(\frac{r}{L}\right)^3 \tag{6}$$

for $r \leqslant L$, but it is much more complex for $r > L$. Porod [36] has attempted to formulate general rules for how $\gamma_0(r)$ depends on the shape but it

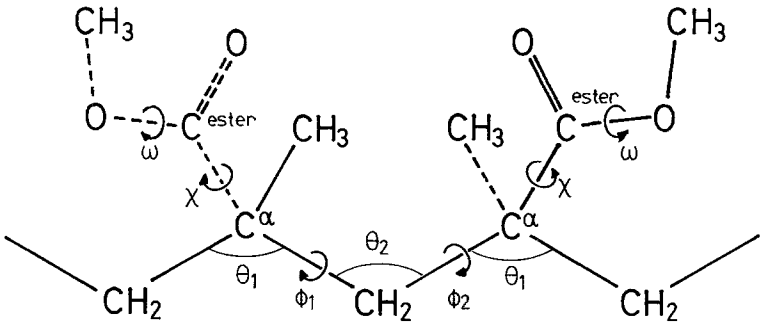

Figure 6 Representation of the chemical structure of a racemic dyad of PMMA, the basic unit of the model chains. All rotation angles are shown as zero.

seems that, for our purposes, using $\gamma_0(r)$ is only suitable for a spherical model.

As the single chains we are modelling are generally nowhere near spherical, we have adopted a different approach. This is to smear out the features of the broadened histogram still further so that only the general shape remains. We found that a Gaussian smearing function with a standard deviation of 0.08 nm was adequate for this. The fully smeared form is shown as the dashed line in Fig. 5b. The difference between the two curves is plotted in Fig. 5c and is the reduced RDF of a finite single chain of PMMA. Since this work was completed, a more exact, less empirical procedure for deriving the shape function has been developed [38].

6. Comparison of experimental RDF of PMMA with model RDFs

The main conclusion of our earlier work on PMMA [15] was that the conformation is close to all-trans but with a marked difference between the alternate backbone bond angles θ_1 (at the substituted carbon atom). and θ_2 (at the methylene carbon atom), giving a curved backbone. We have in general confirmed this conclusion by comparing the positions of peaks in model RDFs with those of the experimental RDF. The prominent peaks in the experimental RDF (Fig. 3) at 0.67 nm and 0.92 nm are considered first. (The various angles are defined in Fig. 6.)

The model RDFs of Fig. 7a show that the all-trans conformation with $\theta_1 = \theta_2 = 116°$ does not give peaks anywhere near the correct positions. However, a peak close to 0.92 nm can be obtained by decreasing θ_1 to 110° and increasing θ_2 to 122° or more. This peak is, moreover, quite insensitive both to departures from all-trans of 20° or so, and to changing χ, the side group rotation angle, from 0° to 180°.

The peak at 0.67 nm is much more sensitive to conformation and Figs 7 and 8 show that its presence requires χ to be predominantly 180°, with θ_2 in the range 122° to 128° and ϕ between 0° and 10°. This peak mainly represents distances between alternate sidegroups which move apart as the difference between θ_1 and θ_2 causes the backbone to curve. The difference in peak position apparent between conformations with $\chi = 0$ and 180° is because $\chi = 180°$ puts the ester-methyl groups further from the centre of curvature and hence increases the distance between alternate ester-methyls.

A peak near to 0.47 nm is a feature of most of the RDFs in Figs 7 and 8. A substantial contribution to this peak comes from the conformationally insensitive distances between the α-methyl and ester-methyl groups of the same monomer unit. The fact that such a relatively small peak is also seen in the experimental RDF elicits confidence in the general procedure. The experimental peak at 0.34 nm appears in few of the model RDFs, most conformations giving a peak between 0.36 and 0.37 nm. In fact, only for model conformations with $\theta_2 = 128°$ and $\phi = 10°$ to 20° is there a peak in the correct position. Consideration of all the peaks in the experimental RDF confirms that the conformation is close to that put forward on the basis of comparisons between experimental and calculated scattering [15], that is (10°, 10°, −10°, −10°) with $\theta_1 = 110°$ and $\theta_2 = 128°$ although, on the basis of this RDF analysis it appears that an ester group rotation angle of $\chi = 180°$ is to be preferred. The proposed model is drawn in Fig. 9. The relevance of the curvature of the molecule to the non-crystallizability of bulk syndiotactic PMMA has previously been alluded to [15].

It has not been possible on the basis of this RDF analysis to refine the estimate of the run

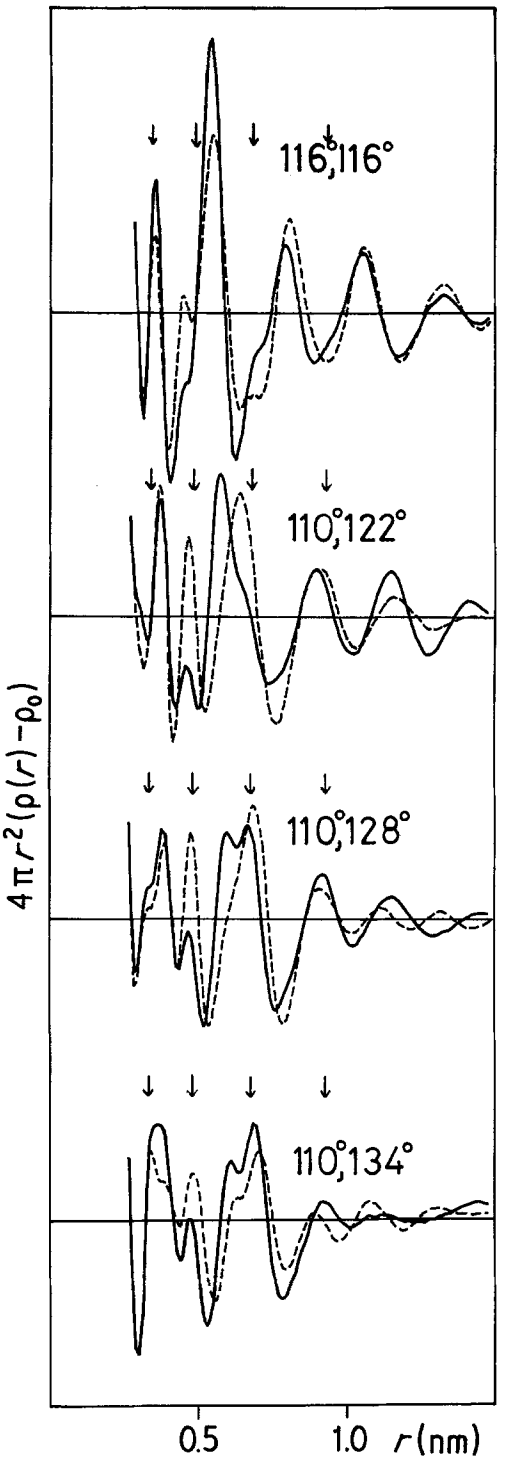

Figure 7 RDFs calculated from models of PMMA illustrating the effect of changing backbone bond angles. The backbone rotation angles are held at zero. In each case the calculation has been made for two settings of the side group rotation angle, at $\chi = 0°$ (continuous line) and $\chi = 180°$ (dashed line). The arrowheads show the position of the four main intra-chain experimental peaks.

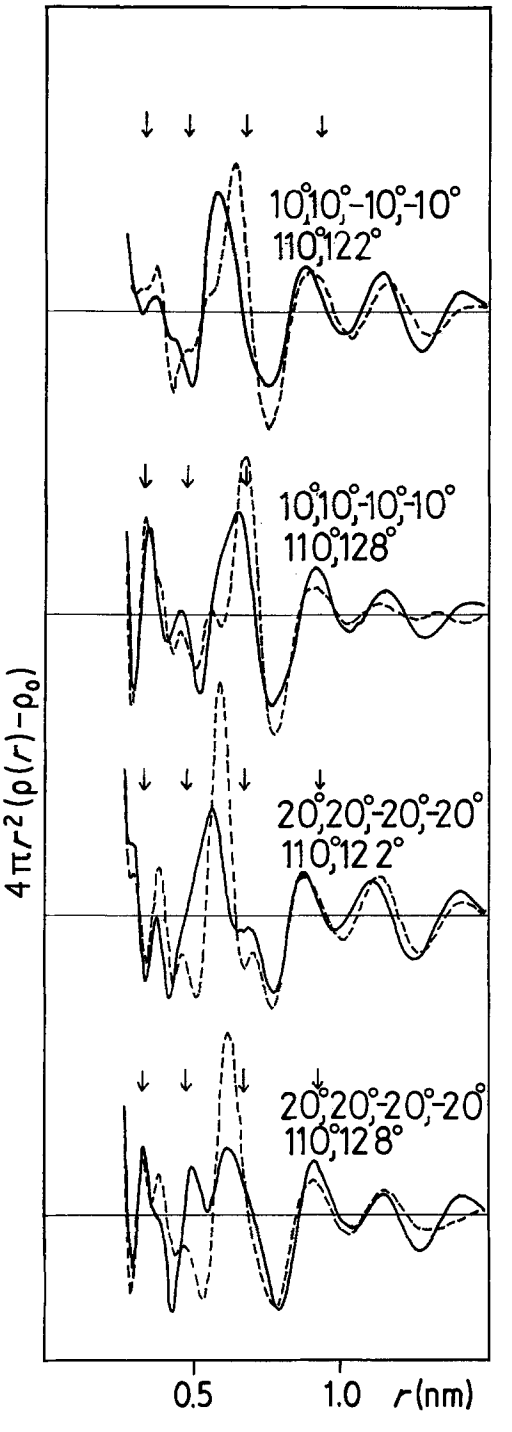

Figure 8 RDFs of models of PMMA chains with backbone bonds rotated away from all-trans by 10° and 20° in the sequence $(+\phi_1, +\phi_2, -\phi_1, -\phi_2)$. The curves have been calculated for two sets of bond angles $(\theta_1, \theta_2) = (110°, 122°)$ and $(110°, 128°)$, and for $\chi = 0°$ and 180° as above. Again, the arrowheads indicate positions of experimental peaks.

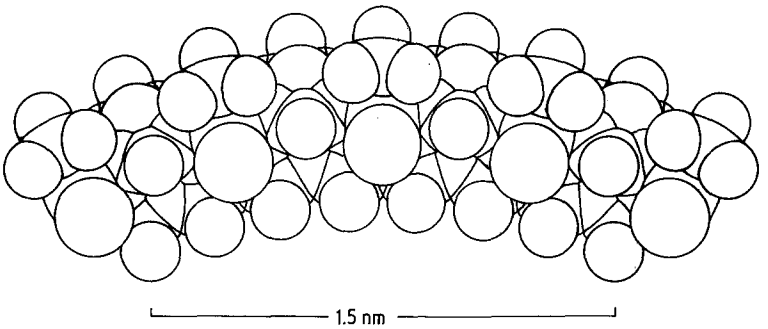

Figure 9 Drawing of a segment of a syndiotactic PMMA chain in the proposed conformation.

length of this underlying conformation made earlier [14, 15]. Since estimates of the length can only be derived from a RDF by precise comparison of relative peak heights, a more reliable measure may be obtained by analysis of the widths and shapes of peaks in the interference function.

In Fig. 10 we compare the RDF for the proposed conformation with RDFs for three conformations which have been proposed earlier as a result of energy calculations. It can be seen that these earlier proposals give RDFs which are in poor agreement with experiment. Even the conformation proposed by Sundararajan and Flory [31], which gives scattering in good agreement with experiment, gives a relatively poor fit to the RDF. This demonstrates an apparently superior sensitivity of the RDF analysis, even though the experimental information can be no more than that in the measured scattering.

7. Conclusions

An RDF has been prepared from X-ray scattering data from atactic PMMA. The data were collected using an energy dispersive detector, which eliminated the need for independent calculations of the Compton component and multiple scattering. The errors present in the RDF have been examined and where possible assessed quantitatively. It is held that the RDF presented is free from spurious features of any kind.

On the basis of comparisons between experimentally determined RDFs and similar functions calculated from computer-built models, a conformation is proposed for atactic PMMA. It is: $(\phi_1, \phi_2, \phi_3, \phi_4) = (10°, 10°, -10°, -10°)$, i.e. near all-trans, $\theta_1 = 110°, \theta_2 = 128°$, and $\chi = 180°$.

The advantages that RDF analysis has over comparisons in reciprocal space appear as:

(a) A carefully prepared experimental RDF tends to have more peaks than does the corresponding scattering.

(b) The peak positions in an experimental RDF are insensitive to errors in corrections, since errors in multiplicative corrections convolute the true RDF with a symmetrical function.

(c) A RDF is more sensitive to small conformational changes than is the scattering.

There are also disadvantages:

(a) It can be difficult to separate the RDF into its intra- and inter-chain components but this can be aided by calculating cylindrical distribution functions from oriented specimens.

(b) A considerable amount of data correction and manipulation is needed but almost the same effort is required to obtain reliable reduced scattering, $sZ(s)$.

(c) Changes in regularity or sequence length are reflected in the relative magnitudes of peaks in the RDFs, whereas in the scattering there are distinct and obvious changes in peak shape.

However, although it is possible to contrast data–model comparisons in real and reciprocal space, the approaches are best seen as complementary. In fact, in this structural investigation the RDF analysis and comparison in real space served to confirm and refine the model put forward on the basis of reciprocal space comparisons made in an earlier stage of this work [15].

Acknowledgements

The authors are grateful to Professor R. W. K. Honeycombe for the provision of facilities, to the SERC for funding via a grant (GR/A 13387) and a studentship (JRW) and to Robert Collins and Mike Smith for general laboratory assistance.

Appendix 1: Brief review of RDF procedure

The method of RDF analysis has been extensively reviewed, for example [22], so the purpose of this brief sketch is one of convenience in that it

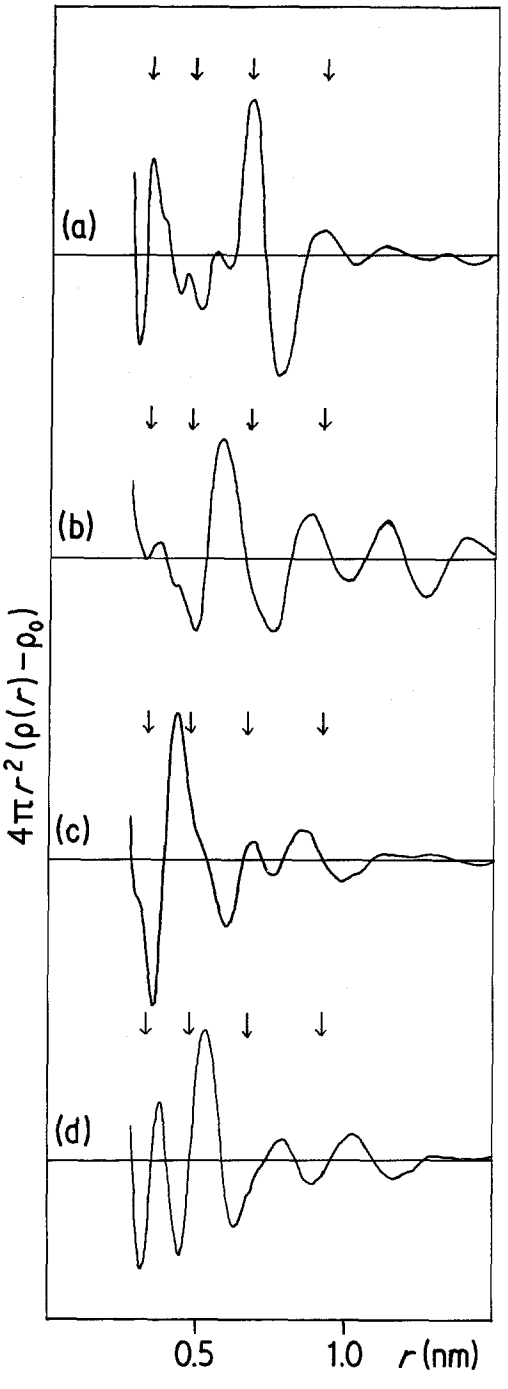

Figure 10 A RDF (a) calculated for proposed conformation (arrowheads show experimental peak positions). (b) calculated for a model of the model of Sundararajan and Flory [31]. $\phi s = (10, 10, -10, -10)$, $(\theta_1, \theta_2) = (110°, 112°)$, $\chi = 0°$. (c) from the first model of Grigovera *et al.* [39]. $\phi s = (0, 150, 0, -150)$; $(\theta_1 = \theta_2) = (114°)$, $\chi = \pm 30°$. (d) from the second model of Grigovera *et al.* [40] $\phi s = (10, 10, -10, -10)$, $(\theta_1 = \theta_2) = (114°)$, and $\chi = 0°$.

outlines the actual method used in this work as well as defining the symbols used.

Before the experimental scattering data can be transformed to give a RDF it must be both corrected and reduced. For X-radiation, correction must be made for polarization, multiple scattering and absorption; and as the RDF is derived from coherently scattered radiation, the incoherent (Compton) component must be removed. Usually the Fourier transformation is carried out on the s-weighted reduced intensity function ($sZ(s)$, $s = 4\pi\sin\theta/\lambda$). This is derived by normalizing the corrected experimental intensity to the independent scattering of an individual atom (Σf^2), averaged over the unit of composition and then subtracting the latter from the normalized data. Compton scattering may also be subtracted at this stage if calculated theoretically and scaled to Σf^2. Hence:

$$Z(s) = kI_{\text{corr}}(s) - \sum_{\text{uc}} f^2(s) - i_{\text{comp}}(s), \quad \text{(A1)}$$

where k is the normalization constant $I_{\text{corr}}(s)$ is the corrected experimental intensity $\Sigma_{\text{uc}} f^2(s)$ is the summation of [atomic scattering factor]^2 over the unit of composition and $i_{\text{comp}}(s)$ is the Compton intensity (calculated).

Normalization has two effects: first, distances between electrons of the same atom are removed from the RDF. Secondly, spurious ripples produced as a result of the abrupt termination at some maximum experimental scattering angle, where the intensity is still significant, are in principle avoided. This is achieved because the experimental scattering and $\Sigma_{\text{uc}} f^2(s)$ can be expected to converge at sufficiently large s giving $Z(s) \to 0$.

X-ray and electron diffraction respond to differences in electron density. Removal of the electron distribution of an average atom by deconvolution converts the electronic RDF ($W(r)$) to an atomic RDF ($G(r)$). Conventionally this is achieved by dividing the function to be transformed by the transform of this electron distribution (Stokes method). The process is usually known as sharpening.

The various steps involved in RDF analysis are summarized in Figs A1 to A9 which also serves as a glossary of the nomenclature used in this paper.

Appendix 2: Removal of known distances from a RDF

A technique has been developed [41] which reduces the swamping effect of the first and

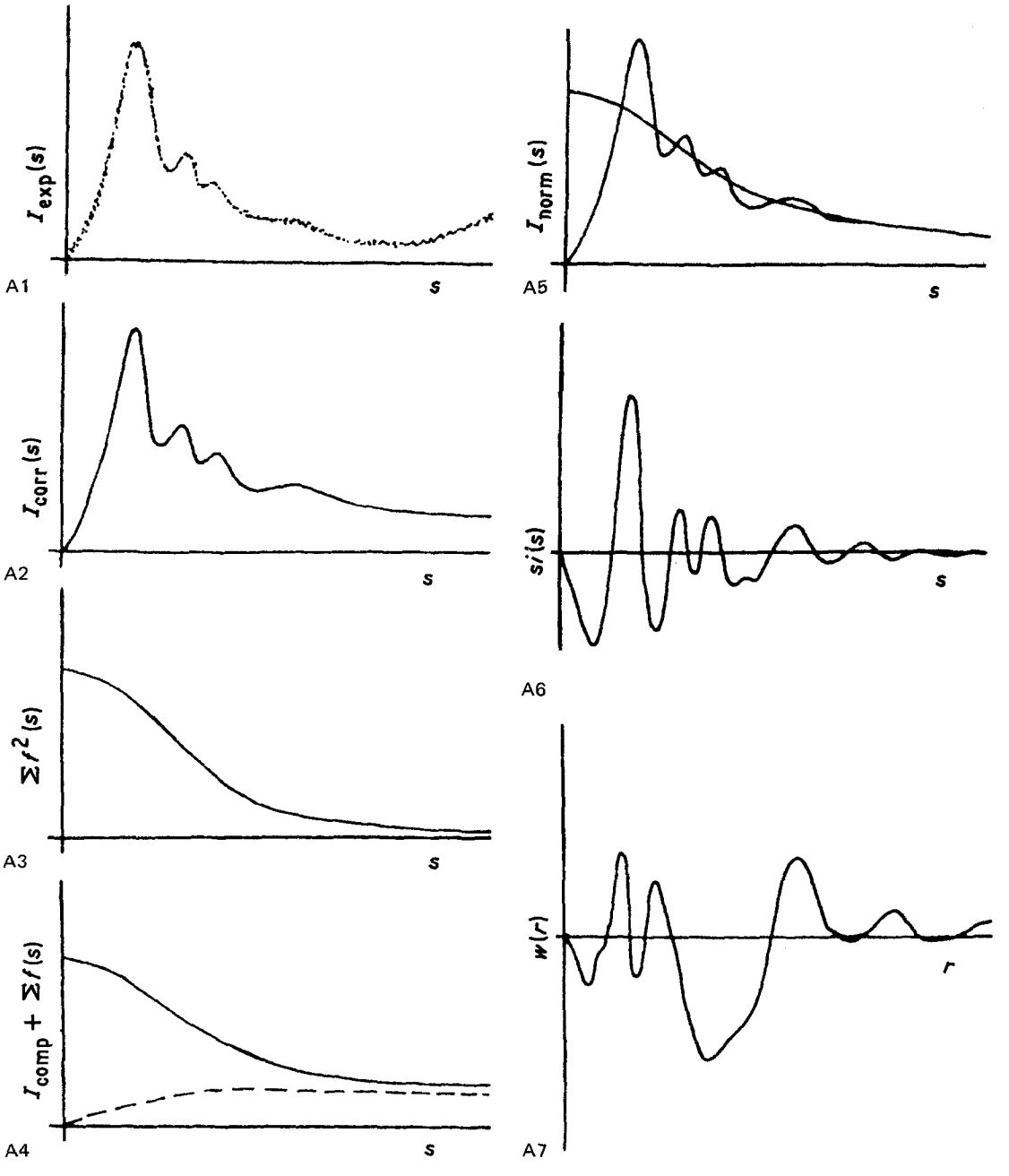

Figure A1 Showing a summary of the steps in the RDF analysis, the raw data.
Figure A2 The raw data is corrected for polarization, absorption and multiple scattering, is smoothed and interpolated to constant Δs.
Figure A3 The independent scattering for an "average" atom in the system being considered is calculated. This is in fact the transform of the distribution of intra-atomic electron–electron distances.
Figure A4 The incoherent (Compton) scattering i_{comp} from an average atom is calculated and added to $\Sigma_{uc} f^2$.
Figure A5 The smoothed and corrected data is scaled to $\Sigma_{uc} f^2 + i_{comp}$ by the normalization procedure.
Figure A6 $Z(s)$, the difference between k times the corrected data and $(\Sigma_{uc} f^2 + i_{comp})$, should oscillate about zero. It is usually known as the interference function. k is the scaling factor (normalization constant).
Figure A7 The distribution of inter-electron vectors except those between electrons in the same atom [the electronic radial distribution function] is given by: $W(r) = 4\pi r(\rho(r) - \rho_0) = \int_0^\infty sZ(s) \sin rs \, ds$. In other words the RDF, $W(r)$, is given by the sine Fourier transform of the s-weighted interference function.

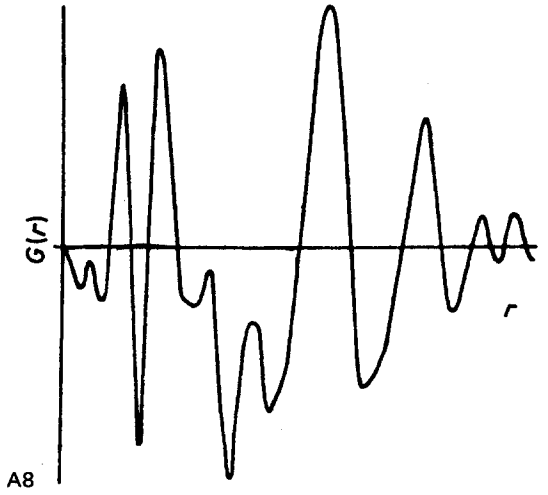

A8

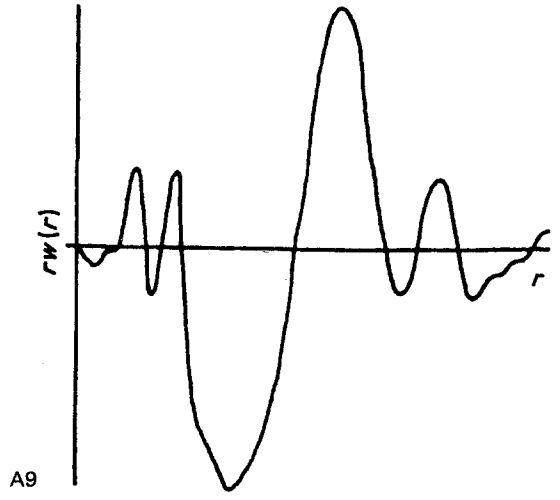

A9

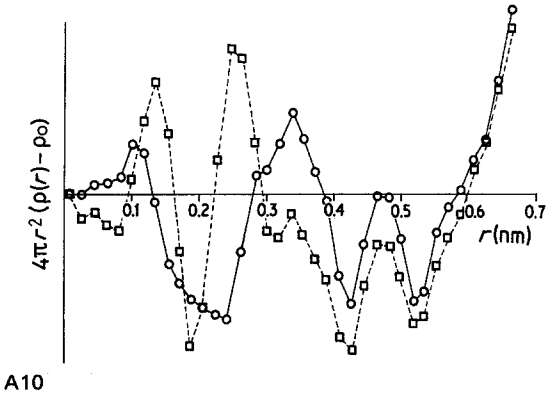

A10

Figure A8 If the distribution of inter-atomic vectors is required, the averaged distribution of electrons about an atom is deconvoluted from $W(r)$ to give the sharpened function $G(r)$, known as the atomic RDF. The sharpening is achieved by dividing the interference function $Z(s)$ by $(\Sigma f)^2$ prior to the Fourier transform. Alternatively $G(r)$ may be obtained by iterative deconvolution of $W(r)$ using the electron distribution of an "average" atom. *Figure A9* The difference between the number of electrons in a spherical shell (of thickness δr, and radius r from an "average" atom) and the average number of electrons in a volume $4\pi r^2\,\delta r$ is known as the radial density function. *Figure A10* RDFs illustrating the effect of removing those inter-atomic distances fixed by the chemical configuration. The dashed line is, in effect, a section of Fig. 3; the full line is the result of removing the known distances (mainly nearest and next nearest neighbours).

second nearest neighbour distances and which is particularly applicable to unsharpened functions and those derived from data over a limited range of s (e.g. using CuKα radiation). It involves normalizing the corrected data to $\Sigma_{uc} f^2(s)$ modulated by a function representing the interferences due to the first and second nearest-neighbour distances calculated with a knowledge of the chemical structure.

The process effectively removes the first two large peaks in the RDF. It corresponds to the removal of electron density from the relevant region of the RDF. Hence, in order to avoid a large "hole" the transform of a sphere of uniform atomic density and equivalent scattering power, $H(s)$, [35] is also subtracted from the modulated independent scattering, $[\Sigma_{uc} f^2(s)]_m$, given by

$$\left[\sum_{uc} f^2(s)\right]_m = \sum_i \sum_j f_i f_j \frac{\sin sr_{ij}}{sr_{ij}} - H(s). \quad \text{(A2)}$$

Only r_{ij} values defined by the chemical structure are used but each appears twice, and

$$H(s) = \frac{9(N\Sigma f)^2}{(Rs)^6}\,[\sin(Rs) - Rs\cos(Rs)], \quad \text{(A3)}$$

where R is the radius of the depleted volume and N is the number of atoms removed from the volume.

The consequence of applying this procedure to the data for PMMA is shown in Fig. A10, where the peaks at $r = 0.33$ and 0.47 nm are more clearly defined.

Appendix 3: General guidelines for the assessment of quality of a RDF

These are suggested in the context of non-crystalline polymers, but are mostly applicable to non-crystalline materials in general. To some extent they appear self-evident, but it is clear from the literature that misinterpretation can occur if they are not given due regard.

A3.1. Function plotted

Perhaps not surprisingly, a RDF plotted as $4\pi r(\rho(r)-\rho_0)$ can emphasize features which are not so apparent on a $4\pi r^2(\rho(r)-\rho_0)$ plot and vice versa. Also an atomic RDF generated from data with a high range of s will give peaks for covalently bonded distances which are very sharp and correspondingly intense. Scaling these within the bounds of a graph can mean that important features at higher values of r appear relatively less significant than in RDFs of lower resolution. In this context it is instructive to compare two high resolution atomic RDFs generated from electron diffraction data of molten polythene which have different weightings [9, 10] with a lower resolution electronic RDF of the same material [13].

A3.2. Sharpness of features

The resolution of a RDF is limited by the s_{max} of the data; thus if any feature is sharper than a sinusoidal variation of wavelength $2\pi/s_{max}$ then the analytical procedure should be treated with suspicion. Such false detail will not arise if the RDF is calculated at intervals appropriate to the inherent resolution. In particular, the employment of Kaplow's method [42] and variants [43], where data beyond s_{max} are calculated in order to avoid termination error, can lead to artificially enhanced resolution. This is evident where the method has been applied to polymers [6].

A3.3. General appearance

The appearance of any relatively short wavelength ripple in a RDF of an amorphous material should be viewed with disquiet, for it can only result from sharp features in the data at high values of s. The most common source of ripples is the abrupt termination step at s_{max}. However, methods such as sampled transforms have largely overcome this problem.

In general the RDF of an amorphous polymer will gradually damp towards zero with increasing r [for $4\pi r^2(\rho(r)-\rho_0)$ plots] and the peaks become correspondingly broader.

References

1. S. M. WECKER, T. DAVIDSON and J. B. COHEN, *J. Mater. Sci.* 7 (1972) 1249.
2. G. L. SIMARD and B. E. WARREN, *J. Amer. Chem. Soc.* 58 (1936) 507.
3. A. BJØRNHAUG, Ø. ELLEFSEN and B. A. TØNNESEN, *J. Polymer Sci.* 12 (1954) 621.
4. G. D. WIGNALL and G. W. LONGMAN, *J. Mater. Sci.* 8 (1973) 1439.
5. G. W. LONGMAN, R. P. SHELDON and G. D. WIGNALL, *ibid.* 11 (1976) 1339.
6. M. R. GUPTA and G. S. Y. YEH, *J. Macromol. Sci. Phys.* 15 (1978) 119.
7. G. W. LONGMAN, G. D. WIGNALL and R. P. SHELDON, *Polymer* 17 (1976) 485.
8. O. YODA, I. KURIYAMA and A. ODAJIMA, *J. Appl. Phys.* 49 (1978) 5468.
9. I. VOIGHT-MARTIN and F. C. MIJLHOFF, *ibid.* 47 (1976) 3942.
10. Yu. K. OVCHINNIKOV, G. S. MARKOVA and V. A. KARGIN, *Polymer Sci. USSR* 11 (1969) 369.
11. G. R. MITCHELL and A. H. WINDLE, *J. Appl. Cryst.* 13 (1980) 135.
12. R. LOVELL, G. R. MITCHELL and A. H. WINDLE, *Acta. Cryst.* A35 (1979) 598.
13. G. R. MITCHELL, R. LOVELL and A. H. WINDLE, *Polymer* 21 (1980) 989.
14. R. LOVELL, G. R. MITCHELL and A. H. WINDLE, *Faraday Disc.* 68 (1980) 46.
15. R. LOVELL and A. H. WINDLE, *Polymer* 22 (1981) 175.
16. G. D. WIGNALL, R. N. ROTHON, G. W. LONGMAN and G. R. WOODWARD, *J. Mater. Sci.* 12 (1977) 1039.
17. M. DIXON, A. C. WRIGHT and P. HUTCHINSON, *Nucl. Instrum. Methods* 143 (1977) 379.
18. M. E. MILBERG, *J. Appl. Phys.* 29 (1958) 64.
19. International tables for X-ray Crystallography, (Kynoch Press, Birmingham, 1974).
20. B. E. WARREN and R. L. MOZZI, *Acta Cryst.* 21 (1966) 459.
21. G. R. MITCHELL and R. LOVELL, *ibid.* A37 (1981) 189.
22. A. J. LEADBETTER and A. C. WRIGHT, *J. Non-Cryst. Solids* 7 (1972) 23.
23. *Idem, ibid.* 7 (1972) 141.
24. J. H. KONNERT and J. KARLE, *Acta Cryst.* A29 (1973) 702.
25. H. P. KLUG and L. E. ALEXANDER, "X-ray Diffraction Procedures" (John Wiley and Sons, New York, 1974) Chap. 12.
26. B. E. WARREN and R. L. MOZZI, *J. Appl. Cryst.* 3 (1970) 59.
27. G. S. CARGILL, *ibid.* 4 (1971) 277.
28. A. BIENENSTOCK, *J. Chem. Phys.* 31 (1959) 570.
29. J. P. RYCKAERT and A. BELLEMANS, *Faraday Disc.* 66 (1978) 95.
30. M. VACATELLO, G. AVITABILE, P. CORRADINI and A. TUZI, *J. Chem. Phys.* 73 (1980) 548.
31. P. R. SUNDARARAJAN and P. J. FLORY, *J. Amer. Chem. Soc.* 96 (1974) 5025.
32. B. E. WARREN, "X-ray Diffraction" (Addison-Wesley, Reading, Mass., 1969) Chap. 10.
33. J. WASER and V. SCHOMAKER, *Rev. Mod. Phys.* 25 (1953) 671.
34. A. C. WRIGHT, in "Advances in Structure Research by Diffraction Methods", edited by W. Hoppe and R. Mason (Pergamon Press, Oxford, 1974) p. 1.
35. A. GUINIER and G. FOURNET, "Small-angle Scattering of X-rays" (John Wiley and Sons, New York, 1955) Chap. 2.

36. G. POROD, in "Small-angle X-ray Scattering" edited by H. Brumberger (Gordon and Breach, New York, 1967) p. 1.
37. R. J. BELL, *Nature* **218** (1968) 985.
38. G. R. MITCHELL, *Acta Cryst.* **A37** (1981) 488.
39. F. P. GRIGOREVA, T. M. BIRSHTEIN and Yu. Ya. GOTLIB, *Polym. Sci. USSR.* **9** (1967) 650.
40. *Idem. Ibid.* **10** (1968) 396.
41. J. R. WARING, PhD thesis, Cambridge, (1979).
42. R. KAPLOW, S. L. STRONG and B. L. AVERBACH, *Phys. Rev. A* **138** (1965) 1336.
43. A. D'ANJOU and F. SANZ, *J. Non. Cryst. Solids* **28** (1978) 319.

Received 21 August
and accepted 19 September 1981